Supporting Information

Denker et al. 10.1073/pnas.1112690108

SI Discussion

We summarize here some of the basic features of buffers, as well as order of magnitude estimates for buffer-related quantities, such as buffering ratio and geometric constraints.

Section 1: Lower Bound to the Concentration of Free Clathrin, [*X*]. To define the demands on a localized (clustered) buffer, we first need to estimate the strength of the molecular sink, which the buffer has to cope with (the sink in this case being formed by the clathrin-coated objects that sequester clathrin). We assume that the formation of a clathrin coat requires n sequential steps of a given binding reaction (such as addition of a clathrin triskelion to a coated pit) and that the whole process should be completed in t seconds. The individual steps cannot be faster than the mean waiting time until a ligand hits the binding site. The theory of diffusion-limited reactions (1) gives an expression for the diffusion-limited second order reaction rate constant k of a particle hitting a flat surface element with radius r:

$$k = \frac{2\pi N D r}{1000}, \qquad \text{[S1]}$$

where N is Avogadro's number, and D is the diffusion coefficient of the diffusing particle. The number 1,000 in the denominator is required for obtaining the result in units of $M^{-1}s^{-1}$, when D and r are entered in cgs-units. Taking as r a value of $5\cdot10^{-8}$ cm, which is typically used for enzymatic reactions, and for D a value of $3\cdot10^{-8}$ cm^2/s, which is one quarter of the value measured for clathrin triskelia (2), taking into account viscosity and crowdedness of cytosol, one arrives at: $k = 5.7\cdot10^6$ $M^{-1}s^{-1}$.

To reach a rate of ν ($=k\cdot[X]$) events per second, the required concentration $[X]$ of free molecules is given by the condition:

$$[X] = \frac{\nu}{5.7\cdot10^6}. \qquad \text{[S2]}$$

Assuming that clathrin coats form at a rate of approximately one per second (see main text) and that this involves approximately five sequential binding steps [triskelia binding occurs at several sites in parallel to form a coated vesicle with approximately 50 triskelia (3)], we can postulate a binding rate for an individual site of approximately five per second and arrive at ≈1 μM for the minimum concentration of free triskelia. This concentration is required to deliver a sufficient number of units at this rate in case the reaction is diffusion-limited.

Section 2: Influence of Synapse Geometry on Buffering Properties. If we postulate that at least half of the molecules should at any one time be available within reach of the sites of demand (i.e., within the boutons), the buffering ratio κ should be:

$$\kappa > \frac{v_{tot}}{v_{bouton}}, \qquad \text{[S3]}$$

where v_{tot} is the accessible volume of the whole cell, apart from the synaptic boutons, and v_{bouton} is the volume of the latter.

Considering a frog neuromuscular junction (NMJ) axon with an effective length of approximately 850 μm (the diffusional distance that the molecule can cover within its own lifetime, assuming it to be ≈10 h, under linear diffusion with a diffusion coefficient of 10 $\mu m^2/s$; see above), a volume ratio of ≈230 is obtained, given the known diameters and lengths of frog NMJ axons and synapses. Thus, κ should be in the range of several hundred to fulfill the requirement that the majority of protein should be located near its site of use. The value is much lower for the hippocampal culture, where the bouton volume [0.12 μm^3 (4)] is only approximately eight times smaller than the volume of a typical axon length between boutons (assuming a length of ≈5 μm and a diameter of ≈0.5 μm).

However, how large is the tolerable distance between the reservoir and the site of use? Postulating that diffusion time should not be longer than the reaction time (0.2 s), we can calculate for 3D diffusion ($\bar{x}^2 = 6Dt$) a distance between 1.9 μm (using the above diffusion coefficient, $3\cdot10^{-8}cm^2s^{-1}$) or else 0.6 μm (using the experimentally determined value of $\approx3\cdot10^{-9}$ cm^2s^{-1} from ref. 5).

Section 3: Calculation of Buffering Ratio. Here we analyze fluorescence ratios (bouton vs. axonal fluorescence) as given for several proteins in Fig. 2 (main text). We assume—also for simplicity—that a given voxel extends through the structure of interest (bouton or axon). With the geometrical definitions given in *SI Discussion, Section 2* we can write for the measured fluorescence ratio F_{bouton}/F_{axon} for a pixel in the center of the respective structure:

$$\frac{F_{bouton}}{F_{axon}} = \frac{[CX]d_{cluster} + [X]d_{bouton}}{[X]d_{axon}}.$$

We split d_{bouton} (the length across a bouton) into a sum: $d_{cluster}+d_{void}$, where $d_{cluster}$ is the cluster length and d_{void} is the length across a bouton, not covered by a cluster, and arrive at:

$$\frac{F_{bouton}}{F_{axon}} = (\kappa+1)\frac{d_{bouton}}{d_{axon}} + \frac{d_{void}}{d_{axon}},$$

where κ is the buffering ratio, as defined in Eq. **5** (main text); see also Eq. **S3**.

We determine the fluorescence ratio both under control conditions and after treatment with black widow spider venom (BWSV). The ratio R of both values is then:

$$R = \frac{(\kappa_c+1)\frac{d_{bouton}}{d_{axon}} + \frac{d_{void}}{d_{axon}}}{(\kappa_{BWSV}+1)\frac{d_{bouton}}{d_{axon}} + \frac{d_{void}}{d_{axon}}}.$$

It is understood that the geometric parameters in nominator and denominator refer to the respective geometries, which may change during BWSV treatment. Rearranging and introducing

$$r_c \equiv \left.\frac{d_{void}}{d_{bouton}}\right|_{control}$$

$$r_{BWSV} \equiv \left.\frac{d_{void}}{d_{bouton}}\right|_{BWSV},$$

we obtain:

$$R = \frac{(\kappa_c+1)+r_c}{(\kappa_{BWSV}+1)+r_{BWSV}}$$

or

$$\kappa_c = R\{\kappa_{BWSV} + 1 + r_{BWSV}\} - (r_c + 1).$$

Considering reasonable numbers ($R \approx 5$; r_c and $r_{BWSV} < 1$), κ_c has at least a value close to $2 \times R$ (for $\kappa_{BWSV} = 0$ and $r_{BWSV} \approx 1$). Several times this value is obtained if κ_{BWSV} is >1. Thus, we take $2 \times R$ as a lower bound for κ_c (as given in Table S1 for the different proteins investigated).

SI Methods

Unless stated otherwise, all chemicals were purchased from Merck, Sigma, or VWR.

Buffers. Mouse Ringer (6): NaCl 154, KCl 5, $CaCl_2$ 2, $MgCl_2$ 1, glucose 11, and Hepes 5 (pH 7.3) (all concentrations are in mM).

For Ca^{2+}-free buffer, $CaCl_2$ was replaced with $MgCl_2$ and 1 mM EGTA was added.

Electrical Stimulation. Preparations were stimulated using a platinum plate field stimulator (custom-made in the workshop of the Max-Planck Institute for Biophysical Chemistry, Göttingen, Germany) at 100-mA shocks, for 1 min at 30 Hz (for investigation of the effect of ionomycin on exocytosis, Fig. 3*D* in main text) or for 5 min at 30 Hz (Fig. 3 *A* and *B*, main text), using an A385 stimulus isolator and an A310 Accupulser stimulator (World Precision Instruments).

BWSV Treatment/Immunostaining. Two venom glands from *Latrodectus mactans* were homogenized in 1 mL Ca^{2+}-free mouse Ringer using a 1-mL Teflon glass homogenizer (10 strokes at 700 rpm). The preparation was then centrifuged at 20,000 × *g* in a cooled tabletop centrifuge for 5 min (at 4 °C), and the supernatant was removed and kept on ice. One *levator auris longus* muscle was dissected from each mouse investigated (dissected as described in ref. 6). Each muscle was cut longitudinally in two halves, which were pinned in independent dishes: one to be used as control, and one to be used for BWSV incubation. For simplicity, the halves will be referred to as "muscles" below. Normal mouse Ringer (containing Ca^{2+}) or BWSV-containing Ringer was added to the muscles, and the dishes were placed in an incubator at 37 °C for 2 h. Afterward, the muscles were briefly washed in Ca^{2+}-free mouse Ringer. All muscles were then fixed in 4% paraformaldehyde (in PBS) for 60 min and quenched with 100 mM ammonium chloride (in PBS) for 30 min. Muscles were then washed in PBS, followed by permeabilization [3 × 15 min PBS + 0.5% Triton X100 + 2.5% BSA (AppliChem)]. Muscles were incubated for 2 h at room temperature with the following antibodies (typically 1:100 dilution in PBS + 0.5% Triton X100 + 2.5% BSA, from 1 mg/mL stocks in PBS): anti-synaptophysin 1 guinea pig polyclonal, anti-synapsin 1/2 rabbit polyclonal, anti-Rab3 rabbit polyclonal, anti-complexin 1/2 rabbit polyclonal, anti-CSP rabbit polyclonal, anti-NSF rabbit polyclonal, anti-RIM2 rabbit polyclonal, anti-dynamin 1/2/3 rabbit polyclonal, anti-endophilin rabbit polyclonal, anti-synaptojanin 1 C terminus rabbit polyclonal, anti-amphiphysin 1 rabbit polyclonal, anti-AP180 rabbit polyclonal (all from Synaptic Systems), anti-rabphilin R44 rabbit polyclonal (kindly provided by Prof. Reinhard Jahn, Max-Planck Institute for Biophysical Chemistry, Göttingen), anti-clathrin heavy chain mouse monoclonal (BD Biosciences), anti-Hsc70 (B_6) mouse monoclonal (Santa Cruz Biotechnology). Muscles were washed thoroughly in PBS + 0.5% Triton X100 + 2.5% BSA. Muscles were then incubated for 1 h at room temperature with the following secondary antibodies (1:100 in PBS + 0.5% Triton X100 + 2.5% BSA, from 0.5 mg/mL stocks in 50% glycerol): anti-guinea pig donkey polyclonal conjugated to Cy2, anti-rabbit goat polyclonal conjugated to Cy3, and anti-mouse goat polyclonal conjugated to Cy5 (all from Dianova). Muscles were then washed thoroughly in high-salt PBS + 2.5% BSA (500 mM NaCl), followed by normal PBS. The muscles were then mounted in Mowiöl (Calbiochem; prepared as described in ref. 7) between Superfrost slides (Thermo Scientific) and coverslips (Menzel Gläser). The muscles were imaged using an Olympus IX71 microscope equipped with a 20× 0.5 N.A. objective (Olympus) and an F-View II CCD camera (Olympus, 1,376 × 1,032 pixels). Green fluorescence (Cy2) was detected using the 480/40 HQ excitation filter, the 505 LP Q beamsplitter, and the 527/30 HQ emission filter. Orange fluorescence (Cy3) was detected using the 545/30 HQ excitation filter, the 570 LP Q beamsplitter, and the 610/75 HQ emission filter. Red fluorescence (Cy5) was detected using the 620/60 HQ excitation filter, the 660 LP Q beamsplitter, and the 700/75 HQ emission filter (all filters were from Chroma). Illumination was provided by a 100-W Hg lamp (Olympus). On average, terminal diameter was found to increase by ≈50% upon BWSV treatment ($n = 12$ experiments, $P < 0.0001$, *t* test). This would correspond to the fusion of ≈600 vesicles per μm of nerve terminal (or approximately 50% of the vesicles found within 1 μm of a nerve terminal).

Data analysis was performed using software custom-written in MATLAB (MathWorks). Lines were manually drawn along the synapse and onto the axon. Synapses for which the axons were not in focus were ignored. The border between the axon and synapse was manually determined for each synapse. The intensities in the different channels were then calculated, subtracting the background (chosen manually in a region adjacent to the synapse).

The same general experimental protocols were used for investigating the effects of latrotoxin (2 μg/mL), electrical stimulation (30 Hz, 5 min), and ionomycin application (10 μM). EGTA (5 mM) was used in the ionomycin experiments (with Ca^{2+} replaced by Mg^{2+}); control muscles were treated with solvent alone, in identical experiments (0.2% DMSO); the ionomycin experiments were performed at room temperature.

Colocalization Experiment/Immunostaining. *Levator auris longus* muscles were dissected in standard mouse saline. Muscles were fixed, quenched, and permeabilized as described above (*BWSV Treatment/Immunostaining*). The muscles were then incubated for 2 h at room temperature with the following antibodies (typically 1:100 or 1:200 dilution in PBS + 0.5% Triton X100 + 2.5% BSA, from 1 mg/mL stocks in PBS): anti-synaptophysin 1 guinea pig polyclonal, anti-AP180 rabbit polyclonal, anti-complexin 1/2 rabbit polyclonal, anti-CSP rabbit polyclonal, anti-NSF rabbit polyclonal, anti-RIM2 rabbit polyclonal, anti-cortactin mouse monoclonal, anti-tubulin rabbit polyclonal, anti-dynamin 1/2/3 rabbit polyclonal, anti-caveolin rabbit polyclonal, anti-endophilin rabbit polyclonal, anti-amphiphysin 1 rabbit polyclonal, anti-Rab3 rabbit polyclonal, anti-synaptojanin 1 C terminus rabbit polyclonal, anti-synapsin 1/2 rabbit polyclonal (all Synaptic Systems), anti-clathrin heavy chain mouse monoclonal (BD Biosciences), anti-Bassoon mouse monoclonal (Stressgen, Assay Designs), anti-synaptophysin G96 rabbit polyclonal, anti-rabphilin R44 rabbit polyclonal (both kindly provided by Prof. Reinhard Jahn, Max-Planck Institute for Biophysical Chemistry, Göttingen, Germany), anti-Hsc70 (B_6) mouse monoclonal (Santa Cruz Biotechnology). Muscles were washed thoroughly in PBS + 0.5% Triton X100 + 2.5% BSA and incubated for 1 h at room temperature with the following secondary antibodies (1:100 dilution in PBS + 0.5% Triton X100 + 2.5% BSA, from 0.5 mg/mL stocks in 50% glycerol): anti-guinea pig donkey polyclonal conjugated to Cy2 (Dianova), anti-rabbit goat polyclonal conjugated to Atto647N (antibody from Dianova, dye from ATTO-TEC; the antibodies were labeled with the NHS-ester of the dye, as described in ref. 7), and anti-mouse goat polyclonal conjugated to Atto647N (Synaptic Systems). Subsequently, muscles were washed overnight in high-salt PBS + 2.5% BSA. Before embedding in TDE (2,2′-thiodiethanol; Sigma), the muscles were once more

washed with high-salt and normal PBS and subsequently treated with a TDE dilution series (30%, 50%, 70%, and 90% in ddH_2O, 10 min each, followed by 3× 100%, 10 min each).

Muscles were imaged using a Leica TCS SP5 stimulated emission depletion (STED) confocal microscope equipped with a 100× 1.4 N.A. HCX PL APO CS oil objective (Leica). For confocal imaging, the 488-nm line of an Argon laser was used for excitation of the green staining (synaptophysin, Cy2); Atto647N (labeling the protein of interest) was excited using a Helium-Neon laser (633-nm wavelength). For STED mode, excitation of Atto647N was performed using a pulsed diode laser (635 nm), and depletion was achieved via a Spectra-Physics MaiTai tunable laser (Newport Spectra-Physics) at 750 nm. Appropriate emission intervals were selected using an AOTF filter (Leica). Signal detection in confocal mode was performed by photomultiplier tubes and in STED mode by an avalanche photodiode. Images were acquired in the green (synaptophysin) and Atto647N channels in confocal mode, followed by acquisition of the corresponding STED image (Atto647N). Data analysis was performed using software custom-written in MATLAB. Briefly, the STED image was aligned to its corresponding confocal image (Atto647N), and regions of interest (encompassing a synaptic area of at least ≈2 μm in width and several micrometers in length) were defined manually in the images. Pearson's correlation coefficient was determined for the green and STED intensity in each region of interest.

Two-color STED microscopy was performed as previously described (8), using donkey anti-guinea pig polyclonal antibody labeled with Atto590 (for synaptophysin, as a marker for synaptic vesicles) and goat anti-rabbit polyclonal antibody conjugated to Atto647N or goat anti-mouse polyclonal antibody conjugated to Atto647N (all other proteins). For viewing purposes the images were processed using deconvolution filtering.

Biochemical Experiments. Highly purified synaptic vesicles were obtained from rat brain as previously described (9). Either homogenate or synaptic vesicles (7 μg per lane) were investigated by SDS/PAGE/Western blot by conventional methods.

The vesicle pelleting experiments were performed using crude synaptic vesicles (LS1), using an in vitro protocol previously described (10). Synaptic vesicles (crude vesicles, LS1 fraction) were obtained as previously described (11). They were incubated with a mixture containing rat brain cytosol (1 mg/mL, prepared as described in ref. 10), 45 mM potassium acetate, 1.35 mM magnesium acetate, 0.18 mM di-thio-threitol, 11.25 mM Hepes buffer (pH ≈7.3), and either an ATP-regeneration system (26.7 mM creatine phosphate, 3.3 mM ATP, and 13.4 μg creatine kinase) or an ATP-depletion system (15 U hexokinase and 25 mM D-glucose). The quantities described were used in 100-μL volume assay tubes. All protocols and indications on storage and use of the different reagents are provided in ref. 10. Thirty-five micrograms of vesicles were incubated at 37 °C for 30 min with 100 μg of cytosol (in the above-described mix) and the ATP depletion or regeneration systems mentioned; for some experiments 1 mM $CaCl_2$ or 5 mM EGTA were added.

The reactions were then centrifuged in a Sorvall S120AT2 rotor, at 360,000 × *g* for 30 min at 4 °C. For the investigation of specific proteins the pellets were directly removed in SDS-containing sample buffer and blotted by conventional SDS/PAGE/Western blot methods. We generally used the same antibodies for Western blotting as for the immunostaining experiments (see above). Synaptobrevin was blotted using the mouse monoclonal 69.1; the mouse monoclonal 41.1 was used for synaptotagmin (both from Synaptic Systems).

Measurements of band density were performed by custom-written routines in MATLAB. All values were corrected for any variations in the amount of vesicle membrane in the pellets (obtained by immunoblotting for the vesicle transmembrane proteins synaptobrevin, synaptophysin, and synaptotagmin).

Statistics. Values indicate mean ± SEM; numbers (n) show the number of independent preparations. P values refer to Student t tests.

1. Alberty RA, Hammes GG (1958) Application of the theory of diffusion-controlled reactions to enzyme kinetics. *J Phys Chem* 62:154–159.
2. Yoshimura T, Kameyama K, Maezawa S, Takagi T (1991) Skeletal structure of clathrin triskelion in solution: Experimental and theoretical approaches. *Biochemistry* 30: 4528–4534.
3. Cheng Y, Boll W, Kirchhausen T, Harrison SC, Walz T (2007) Cryo-electron tomography of clathrin-coated vesicles: Structural implications for coat assembly. *J Mol Biol* 365: 892–899.
4. Schikorski T, Stevens CF (1997) Quantitative ultrastructural analysis of hippocampal excitatory synapses. *J Neurosci* 17:5858–5867.
5. Mueller VJ, Wienisch M, Nehring RB, Klingauf J (2004) Monitoring clathrin-mediated endocytosis during synaptic activity. *J Neurosci* 24:2004–2012.
6. Angaut-Petit D, Molgo J, Connold AL, Faille L (1987) The levator auris longus muscle of the mouse: A convenient preparation for studies of short- and long-term presynaptic effects of drugs or toxins. *Neurosci Lett* 82:83–88.
7. Willig KI, Rizzoli SO, Westphal V, Jahn R, Hell SW (2006) STED microscopy reveals that synaptotagmin remains clustered after synaptic vesicle exocytosis. *Nature* 440: 935–939.
8. Bückers J, Wildanger D, Vicidomini G, Kastrup L, Hell SW (2011) Simultaneous multi-lifetime multi-color STED imaging for colocalization analyses. *Opt Express* 19: 3130–3143.
9. Takamori S, et al. (2006) Molecular anatomy of a trafficking organelle. *Cell* 127: 831–846.
10. Barysch SV, Jahn R, Rizzoli SO (2010) A fluorescence-based in vitro assay for investigating early endosome dynamics. *Nat Protoc* 5:1127–1137.
11. Rizzoli SO, et al. (2006) Evidence for early endosome-like fusion of recently endocytosed synaptic vesicles. *Traffic* 7:1163–1176.

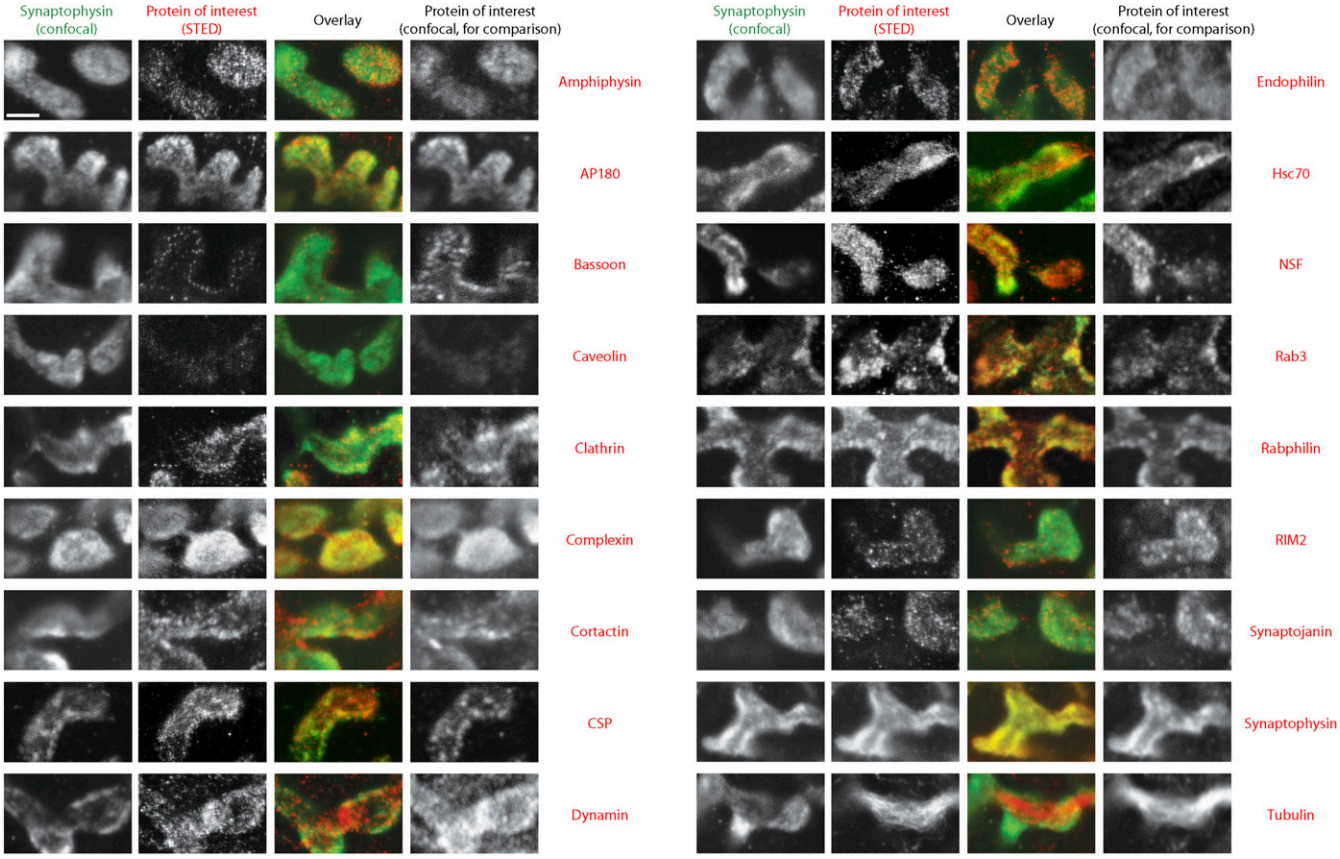

Fig. S1. Synaptic vesicle clusters colocalize with different soluble accessory proteins. Representative mouse NMJ immunostainings for synaptophysin (vesicle marker, confocal mode, *Left*) and all of the proteins of interest that we tested (STED mode, *Center Left*; confocal mode, *Right*). *Center Right*: Overlay of the synaptophysin (green) and STED (red) images. (Scale bar, 2 μm.) The proteins of interest are shown in alphabetical order. Note that most soluble proteins colocalize to different levels with synaptophysin (i.e., amphiphysin, AP180, clathrin, complexin, CSP, dynamin, endophilin, Hsc70, NSF, Rab3, rabphilin, RIM2, synaptojanin). Tubulin and the active zone protein Bassoon provide a lower correlation, whereas caveolin and cortactin may even avoid the vesicle clusters.

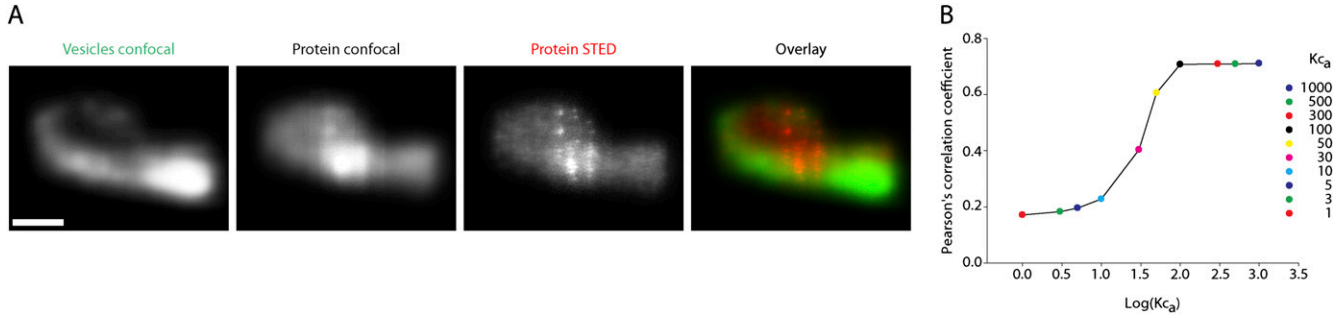

Fig. S2. Modeling the colocalization of synaptic proteins and vesicle clusters. A mathematical model was generated to interpret the fluorescence images from the vesicle cluster-protein of interest colocalization experiments [Fig. 1 (main text) and Fig. S1]. We used a mouse NMJ 3D reconstruction to obtain the distribution of synaptic vesicles in the space of the synapse and the general distribution of the synaptic volume. We then placed fluorescent labels in all of the synaptic vesicles of the reconstruction (n = 4,447) and placed 4,500 virtual proteins in the volume of the synapse. We convolved the vesicle labels with a measured confocal "spot" (point-spread-function), and the proteins with a STED "spot" (obtained from measuring single labeled antibodies on a coverslip with the same microscope used in Fig. 1 and Fig. S1). We then performed virtual sections through the preparation, with the same Z-resolution as in the microscopy experiments, and calculated the correlation coefficient between the two images. To simulate a real situation, a small Z-drift between the images was allowed. The positions of the proteins were simulated 800 times; the graph in *B* shows the mean correlation coefficient. Different protein affinities for the clusters (Kc_a) were simulated. (*A*) Pseudo-fluorescence images for a case in which a Kc_a of 1 (no special affinity for the vesicles, i.e., random protein distribution) is simulated. A confocal image is simulated for the proteins; this is only provided for comparison purposes and was not used in calculations [same as for the real experiments presented in Fig. 1 (main text) and Fig. S1]. (Scale bar, 1 μm.) (*B*) Pearson's correlation coefficient was determined for affinities (Kc_a) ranging from 1 to 1,000. Note that random positioning of molecules results in a correlation coefficient of ≈0.17, whereas an affinity of 1,000 (which results in all molecules bound to synaptic vesicles) provides a correlation coefficient of ≈0.71. Correlation coefficients <0.17 therefore indicate molecules that avoid the vesicles, whereas correlations >0.71 are not possible in this system. The minimum value is higher than 0 (the typical correlation value for random distributions) because although the vesicles and molecules are independently distributed, they all share the same volume, resulting in an overlap of the relevant pointspread functions, which turns into some degree of correlation when performing confocal sections (note that both the STED and confocal images have a confocal Z-resolution). The fact that the maximal correlation is lower than the expected 1 (maximum for Pearson's correlation coefficient) is explained largely by the differences between the diffraction-limited and the STED imaging and by the fact that the positions of the virtual fluorophores on the vesicles are nonidentical, as in a real situation.

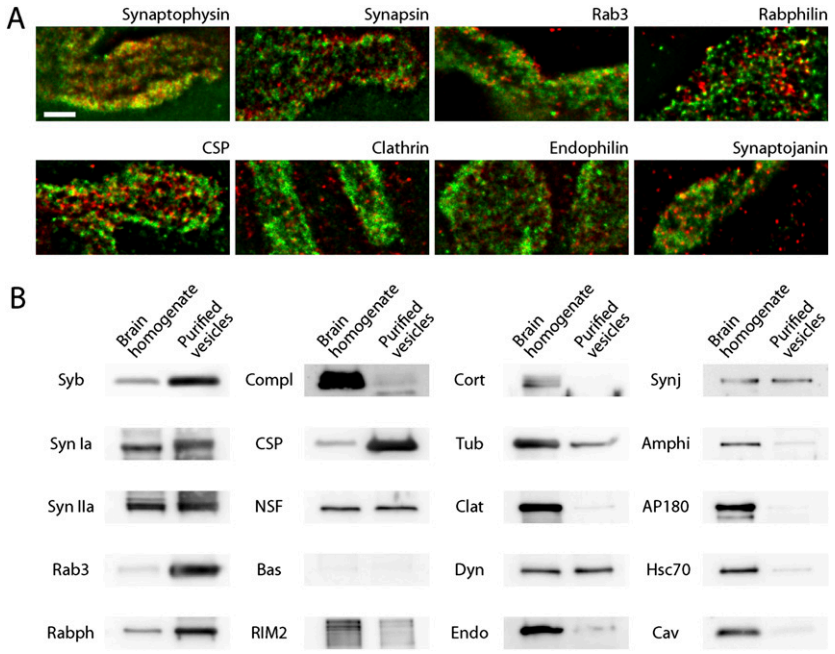

Fig. S3. Further experiments testing the interaction of soluble accessory proteins with synaptic vesicles. (*A*) Two-color STED images of several synaptic proteins. Synaptophysin is shown in green, for all images, with the different proteins of interest shown in red. *Upper Left*: Positive control (synaptophysin labeled with both green and red antibodies). The same phenotype is observed as in Fig. S1: the vesicles form clusters that contain different levels of the proteins of interest. (Scale bar, 1 μm.) (*B*) A variety of soluble proteins are found on synaptic vesicles. We purified synaptic vesicles from rat brain, following the protocol described in ref. 1, which ensures that more than 95% of all analyzed organelles are synaptic vesicles. The blots compare the presence of the different proteins in brain homogenate (*Left*) and in the vesicles (*Right*). The enrichment of the integral synaptic vesicle proteins is indicated by the synaptobrevin blot (Syb; chosen as a vesicle transmembrane protein). Several soluble proteins enrich to similar levels: Rab3, rabphilin, CSP, with a smaller enrichment for synapsin. Synaptojanin, NSF, and dynamin are also present in the vesicle preparation, although they do not seem to be enriched. Several other soluble proteins are found at lower levels, with complexin, for example, found only in trace amounts. Note that this confirms the earlier observation of Takamori et al. (1) that many elements of the clathrin pathway are present to some level on ultra-pure synaptic vesicles.

1. Takamori S, et al. (2006) Molecular anatomy of a trafficking organelle. *Cell* 127:831–846.

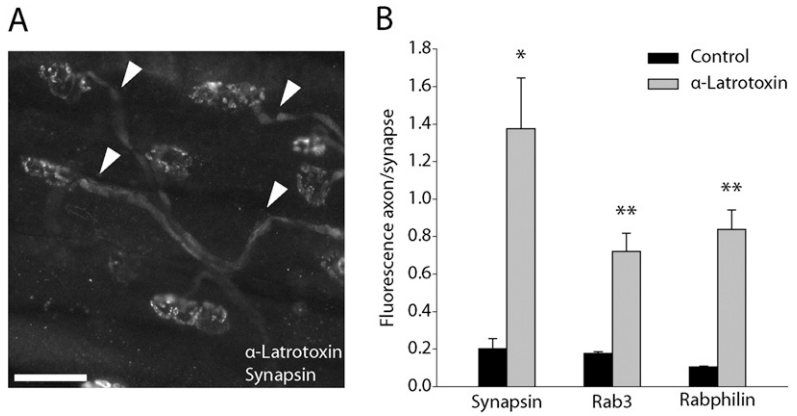

Fig. S4. Latrotoxin reproduces the effects of BWSV treatment. (*A*) To test whether the loss of proteins from the synapses upon BWSV treatment was due to latrotoxin or to other venom components, we incubated preparations with latrotoxin alone (at 2 μg/mL), in the same conditions as for BWSV. Note the high levels of synapsin in the axons, after 2 h of latrotoxin treatment (arrowheads). (Scale bar, 50 μm.) (*B*) Changes in protein distribution after latrotoxin treatment. The ratio of fluorescence within the axon vs. the synapse is shown for control (black) and latrotoxin-treated preparations (gray; three experiments, ±SEM). Asterisks indicate a significant loss of protein into axons (*$P < 0.05$, **$P < 0.01$, *t* test). Note that the values obtained are virtually identical to those from BWSV experiments (Fig. 2 in main text).

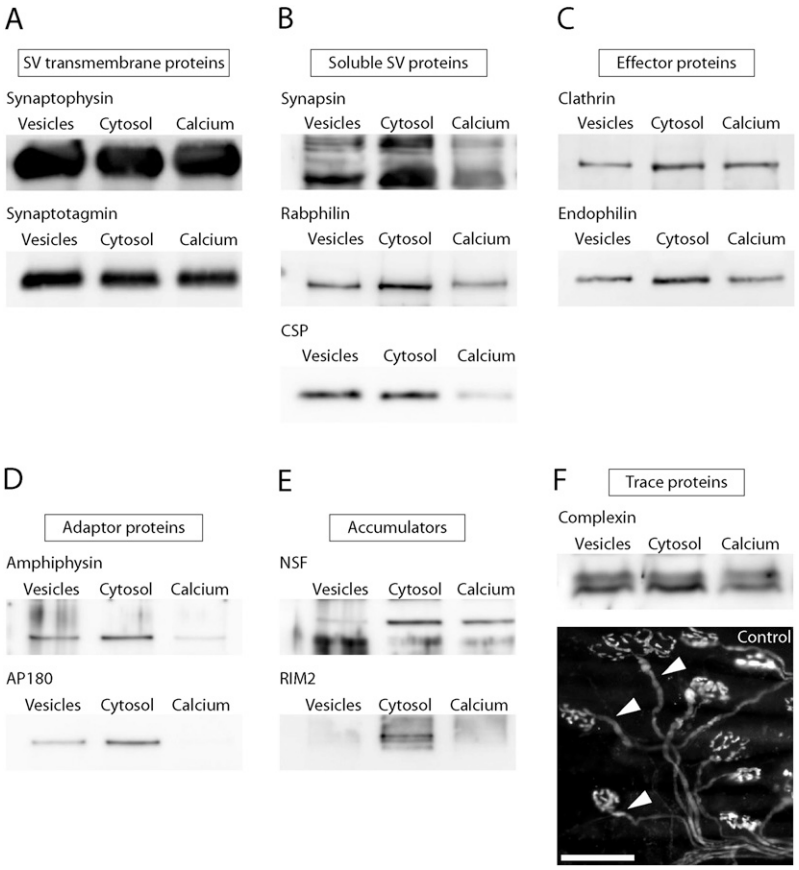

Fig. S5. Investigation of the effects of cytosol and/or calcium addition on protein presence in a vesicular pellet. Representative blots are shown for (*A*) vesicle transmembrane proteins (note that no change is expected). (*B*) Soluble proteins enriched on synaptic vesicles. In the synapsin blot, the bands represent synapsin Ia and IIa. (*C*) Proteins directly involved in endocytosis. (*D*) Endocytosis adaptors. (*E*) Proteins collected in high amounts from the cytosol. The lower bands of the NSF blot represent nonspecific binding of the polyclonal antibody (likely binding to human keratin bands on the blots). (*F*) Complexin (blot reproduced from Fig. 4 in main text, for comparison purposes). Note that complexin is highly abundant in the axons under normal conditions (*Lower*, arrowheads) and therefore should be less affected by protein buffering than other proteins. (Scale bar, 50 μm.)

Table S1. Vesicle clusters bind a plethora of soluble proteins with no apparent function on the clusters, retaining them in the synapse

Protein	Function on vesicle cluster	Localization on vesicle cluster	Loss from synapse upon vesicle depletion (BWSV treatment)	Lower bound for κ (2*R; SI Discussion, Section 3)
Synapsin*	+	+	+	12.3
Rab3[†]	–	+	+	12.4
Rabphilin[‡]	–	+	+	14.6
Complexin[§]	–	+	–	2.8
CSP[¶]	–	+	+	14.2
NSF[‖]	–	+	+	3.6
RIM2**	–	+	+	4.1
Clathrin[††]	–	+	+	4.0
Dynamin[††]	–	+	–	1.2
Endophilin[††]	–	+	–	1.8
Synaptojanin[††]	–	+	–	1.8
Amphiphysin[††]	–	+	–	3.0
AP180[††]	–	+	–	2.1
Hsc70[††,‡‡]	–	+	+	5.8

*Probably tethers synaptic vesicles to each other and the actin cytoskeleton (1). Therefore, is seen as an important molecule in vesicle clustering.
[†]GTPase involved in vesicle exocytosis (2). Disengages from vesicles upon (strong) stimulation and reattaches to them during recovery after stimulation (3).
[‡]Rab effector, binding Rab3 and also calcium. Rabphilin requires Rab3 for binding to synaptic vesicles. Therefore, it will also disengage from vesicles when Rab3 itself unbinds from them (2).
[§]Interacts with SNARE proteins and may be involved in exocytosis (2, 4).
[¶]Secretory cochaperone with multiple functions, mainly in exocytosis (5).
[‖]Member of the AAA protein family (ATPases associated with various cellular activities); involved in SNARE complex dissociation (6).
**Component of the active zone; involved in synaptic vesicle release and plasticity, through interactions with a variety of synaptic proteins, most importantly Rab3 (2, 7).
[††]Components of the clathrin-dependent endocytic machinery (for example, refs. 8–11). Note that the components of this pathway are not expected to leave the synapse upon vesicle depletion (Fig. 2 in main text), because they would tend to bind to the fused synaptic vesicles (11).
[‡‡]ATPase involved in the uncoating of clathrin-coated vesicles (12).

1. Cesca F, Baldelli P, Valtorta F, Benfenati F (2010) The synapsins: Key actors of synapse function and plasticity. *Prog Neurobiol* 91:313–348.
2. Südhof TC (2004) The synaptic vesicle cycle. *Annu Rev Neurosci* 27:509–547.
3. Fischer von Mollard G, Südhof TC, Jahn R (1991) A small GTP-binding protein dissociates from synaptic vesicles during exocytosis. *Nature* 349:79–81.
4. Südhof TC, Rothman JE (2009) Membrane fusion: Grappling with SNARE and SM proteins. *Science* 323:474–477.
5. Evans GJ, Morgan A, Burgoyne RD (2003) Tying everything together: The multiple roles of cysteine string protein (CSP) in regulated exocytosis. *Traffic* 4:653–659.
6. Jahn R, Südhof TC (1999) Membrane fusion and exocytosis. *Annu Rev Biochem* 68:863–911.
7. Mittelstaedt T, Alvaréz-Baron E, Schoch S (2010) RIM proteins and their role in synapse function. *Biol Chem* 391:599–606.
8. Cremona O, De Camilli P (1997) Synaptic vesicle endocytosis. *Curr Opin Neurobiol* 7:323–330.
9. Cremona O, De Camilli P (2001) Phosphoinositides in membrane traffic at the synapse. *J Cell Sci* 114:1041–1052.
10. Slepnev VI, De Camilli P (2000) Accessory factors in clathrin-dependent synaptic vesicle endocytosis. *Nat Rev Neurosci* 1:161–172.
11. Murthy VN, De Camilli P (2003) Cell biology of the presynaptic terminal. *Annu Rev Neurosci* 26:701–728.
12. Zinsmaier KE, Bronk P (2001) Molecular chaperones and the regulation of neurotransmitter exocytosis. *Biochem Pharmacol* 62:1–11.